
DriveAgent-R1: Advancing VLM-based Autonomous Driving with Active Perception and Hybrid Thinking

Weicheng Zheng^{1,3*} Xiaofei Mao^{2*} Nanfei Ye²
Pengxiang Li² Kun Zhan² Xianpeng Lang² Hang Zhao^{1,4†}
¹Shanghai Qi Zhi Institute ²LiAuto ³Tongji University ⁴Tsinghua University

Abstract

The advent of Vision-Language Models (VLMs) has significantly advanced end-to-end autonomous driving, demonstrating powerful reasoning abilities for high-level behavior planning tasks. However, existing methods are often constrained by a passive perception paradigm, relying solely on text-based reasoning. This passivity restricts the model’s capacity to actively seek crucial visual evidence when faced with uncertainty. To address this, we introduce *DriveAgent-R1*, the first autonomous driving agent capable of active perception for planning. In complex scenarios, *DriveAgent-R1* proactively invokes tools to perform visual reasoning, firmly grounding its decisions in visual evidence, thereby enhancing both interpretability and reliability. Furthermore, we propose a hybrid thinking framework, inspired by human driver cognitive patterns, allowing the agent to adaptively switch between efficient text-only reasoning and robust tool-augmented visual reasoning based on scene complexity. This capability is cultivated through a three-stage progressive training strategy, featuring a core Cascaded Reinforcement Learning (Cascaded RL) phase. Extensive experiments on the Drive-Internal dataset, which is rich in long-tail scenarios, and the public nuScenes dataset show that, with only 3B parameters, *DriveAgent-R1* achieves competitive performance comparable to top closed model systems such as GPT-5 and to human driving proficiency while remaining deployment-friendly, offering a proven path toward building more intelligent autonomous driving systems.

Keywords: Autonomous Driving, Vision-Language Models, Hybrid Thinking, Visual Reasoning, Reinforcement Learning

1 Introduction

The paradigm of end-to-end autonomous driving has been substantially advanced by the advent of Vision-Language Models (VLMs) [1, 2, 3, 4, 5]. By emulating human-like cognition, VLMs promise to unify perception, reasoning, and planning within a single, cohesive framework, holding the potential for superior generalization and a deeper understanding of complex scenarios. In the context of planning, the task can be decomposed into two levels: low-level motion planning and high-level behavioral decision-making [6, 1]. Compared to tasking VLMs with regressing continuous physical trajectories—a task for which they are not inherently optimized—a more promising direction is to leverage their strengths in semantic understanding to predict high-level driving intentions [7, 8]. Accordingly, the core objective of this work is to endow agents with the capability for fine-grained, high-level behavioral planning.

To achieve this goal with greater transparency, interpretability, and robustness, we turn to the Multimodal Chain-of-Thought (M-CoT) [9, 10, 11, 12, 13]. The evolution of M-CoT has given

*These authors contributed equally to this work.

†Corresponding at: hangzhao@mail.tsinghua.edu.cn

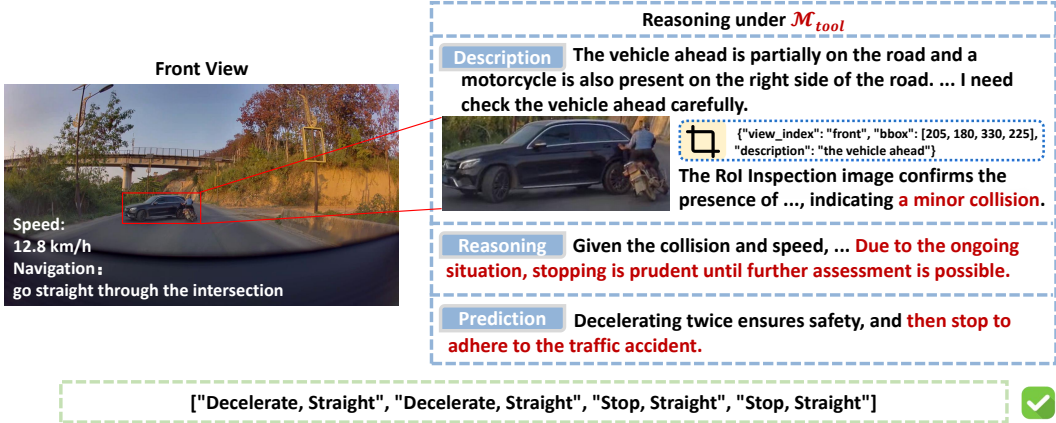


Figure 1: An illustration of *DriveAgent-RI*'s active perception capability. The agent proactively uses RoI Inspection to clarify an uncertain scene, discovering a minor collision between the vehicles ahead. This active perception corrects its initial assessment, leading to a safe plan to decelerate and then stop based on direct visual evidence. More visualization is shown in the Appendix 6.10.

rise to distinct reasoning paradigms: from early Text-based M-CoT [9], which reasons over textual descriptions of visual inputs, to the more sophisticated, interleaved Tool-based M-CoT [13], which actively invokes tools to gather new visual evidence mid-reasoning, enabling a dynamic "think-while-seeing" process. While extensive research has sought to harness M-CoT for autonomous driving tasks [1, 14, 15], these efforts have predominantly remained within the confines of Text-based M-CoT, a paradigm of passive perception. The passive perception struggles with two opposing yet related challenges: (1) it cannot seek additional visual information to resolve ambiguity when the default view is insufficient; and (2) providing comprehensive multi-view data forces the model to process redundant visual inputs, increasing computational overhead and distracting it from critical cues. Human driving, by contrast, is an inherently active process of resolving uncertainty. Drivers will check blind spots or look again at a confusing traffic signal, demonstrating the ability to "actively perceive," which is the cornerstone of safe driving. Tool-based M-CoT provides a technical pathway to instantiate this more human-like driving intelligence, breaking the shackles of passive perception. However, leveraging this tool-based active perception for the core task of high-level behavioral planning remains a significant and unexplored research gap.

While this active perception paradigm is powerful, indiscriminately applying tool-based active perception to all driving scenes is computationally inefficient. Human drivers exhibit a similar cognitive efficiency, relying on intuition for simple conditions and reserving deliberate, active exploration for complex or uncertain scenarios. Such an observation suggests a more intelligent paradigm dynamically adapting its thinking mode: employing efficient Text-based M-CoT for routine cases while deploying the in-depth, Tool-based M-CoT only when the situation's complexity demands it. To our knowledge, such an adaptive mechanism that integrates these distinct M-CoT modalities for the autonomous driving planning task remains unexplored.

To bridge the identified gaps, we introduce *DriveAgent-RI*, a novel autonomous driving agent whose design is centered on two key innovations: active perception and a hybrid-thinking framework. First, it pioneers active perception for high-level behavioral planning. Leveraging a Tool-based M-CoT, *DriveAgent-RI* proactively seeks visual evidence to resolve uncertainty, grounding its decisions in verifiable perception (See Fig. 1). This is enabled by a multi-turn interactive framework centered around a specialized Vision Toolkit, which empowers the agent to acquire diverse visual information on an as-needed basis rather than passively processing redundant multi-view data [16, 17, 18]. Second, we are the first to introduce a Hybrid-Thinking framework to an autonomous driving agent. It innovatively integrates efficient Text-based M-CoT with in-depth Tool-based M-CoT, allowing the agent to adaptively switch its thinking mode based on scene complexity. We cultivate this capability through a three-stage progressive training strategy. Following an initial supervised fine-tuning (SFT) stage, the agent undergoes a novel Cascaded Reinforcement Learning (Cascaded RL) phase. In this core phase, our proposed Mode-Partitioned GRPO (MP-GRPO) algorithm first strengthens each thinking mode individually and then trains the agent to adaptively select the optimal one. On the

Drive-Internal, which features a diverse set of long-tail scenarios, and public nuScenes datasets, our 3B *DriveAgent-R1* achieves performance competitive with top-tier models like GPT-5 [19] and human drivers, while maintaining deployment-friendly efficiency. Crucially, ablation studies confirm this success is genuinely grounded in visual evidence rather than textual shortcuts, validating our active perception and hybrid-thinking framework as a path toward safer, more interpretable autonomous driving. Our main contributions are summarized as follows:

1. We pioneer an **active perception** framework for high-level driving planning. The agent proactively invokes a vision toolkit to ground decisions in visual evidence, enhancing reasoning and reliability.
2. We introduce a **hybrid-thinking framework** that adaptively balances efficient text-only reasoning with robust, tool-augmented visual analysis. This is enabled by a novel **three-stage progressive training strategy** centered on Cascaded RL.
3. *DriveAgent-R1* achieves **both strong performance and deployment-friendly efficiency**. With only 3B parameters, *DriveAgent-R1* proves competitive with top-tier models like GPT-5 and human drivers, while significantly reducing inference latency compared to passive approaches, establishing a practical path toward scalable, intelligent autonomous driving.

2 DriveAgent-R1

2.1 Problem Formulation and Hybrid Thinking

As illustrated in Fig. 2, the agent’s primary task is to generate a long-horizon driving intention sequence from multimodal inputs. Given an initial visual context I_0 (from a front-view camera) and textual context T_0 (vehicle speed and navigation), the agent outputs an 8-second meta-action sequence $A = (a_1, a_2, a_3, a_4)$, with each action predicted at a 2-second interval. Each meta-action $a_t = (s_t, j_t)$ comprises a velocity token $s_t \in V_s = \{\text{Accelerate, Keep Speed, Decelerate, Stop}\}$ and a trajectory token $j_t \in V_j = \{\text{Straight, Right Turn, Left Turn}\}$.

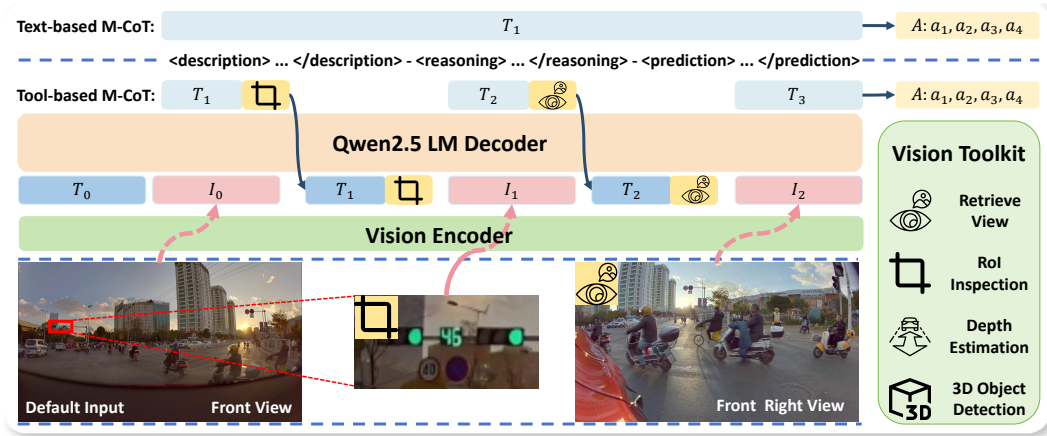


Figure 2: The Hybrid-Thinking architecture of *DriveAgent-R1*. For simple scenarios (Top), the agent uses direct text-based reasoning ($T_1 \rightarrow A$). For complex scenarios (Bottom), it iteratively interleaves thoughts (T_k) with tool calls to a Vision Toolkit, acquiring new visual evidence (I_k) to refine its decision-making. The detailed visualization of this case is shown in Fig. 10, Appendix 6.10.

To achieve this, *DriveAgent-R1* employs a hybrid-thinking mechanism. It first selects a reasoning path by generating either a `<think_text>` or `<think_tool>` token. Both paths adhere to a unified CoT framework: *description*, *reasoning*, and *prediction*, where the *description* stage involves initial perception of the scene, the *reasoning* stage conducts logical analysis, and the *prediction* stage summarizes the analysis to determine the sequence.

Text-based M-CoT ($\mathcal{M}_{\text{text}}$). For common scenarios, *DriveAgent-R1* generates the `<think_text>` token, relying entirely on its internal knowledge and the initial input (I_0, T_0) to make decisions through pure text-based reasoning.

Tool-based M-CoT ($\mathcal{M}_{\text{tool}}$). For complex or uncertain scenarios where the initial visual context is insufficient, *DriveAgent-RI* generates the `<think_tool>` token to engage in active perception, proactively seeking visual evidence to resolve ambiguity and ground its decisions. This process updates its contextual history H_k as follows:

$$H_k = H_{k-1} \oplus T_k \oplus I_k, \quad \text{for } k < K,$$

where $(T_k, \mathcal{T}_k) = \text{LMDecoder}(H_{k-1})$ and $I_k = \text{VisionEncoder}(\text{Execute}(\mathcal{T}_k))$. The process begins with an initial history $H_0 = T_0 \oplus I_0$, where \oplus denotes the concatenation of token embeddings. In each step k , *DriveAgent-RI* generates a textual thought T_k and potentially a tool call request \mathcal{T}_k based on its current history H_k . If a tool is called, it is executed to obtain new visual information, which is then encoded into an image embedding I_k and integrated into the history. The process terminates upon generating the final action sequence A or reaching the maximum interaction limit K .

Vision Toolkit Design. *DriveAgent-RI* is integrated with a powerful Vision Toolkit, endowing it with the capability of active perception. These tools allow the model to explore the environment on demand during its reasoning process to acquire critical information. The toolkit includes: (1) **Retrieve View**, which fetches clear images from any camera, including historical frames from a 5-second memory pool; (2) **RoI Inspection**, a “zoom-in” function that crops and magnifies a specified Region of Interest (RoI) from a higher-resolution image to provide rich visual details; (3) **Depth Estimation**, which generates a depth map to provide crucial 3D spatial awareness; (4) **3D Object Detection**, an open-vocabulary tool that identifies and localizes objects in 3D space. Detailed descriptions and tool call formats are provided in Appendix 6.2.

2.2 Autonomous Driving Domain Alignment

Recent studies [15, 20, 21] indicate that general VLMs exhibit a shortcut tendency in driving planning: they rely on low-dimensional textual cues and neglect high-dimensional visual input. To first develop visual sensitivity and ensure decisions are grounded in evidence, inspired by Drive-R1 [15], we perform autonomous-driving domain alignment on the base model before high-level behavioral planning training. To this end, we build an autonomous-driving VQA dataset from images collected in real traffic, totaling 530K question–answer pairs. Questions in the dataset fall into four main categories: (i) scene description, (ii) recognition of traffic entities, (iii) localization of critical targets, and (iv) traffic commonsense and rules. Using this dataset, we fully fine-tune all parameters of Qwen2.5-VL-3B [22] and obtain *DriveAlign-3B*, a model highly sensitive to visual evidence in driving scenes. *DriveAlign-3B* is used as the unified initialization for the subsequent three-stage training, laying the visual-alignment foundation for *DriveAgent-RI*’s active perception and hybrid thinking. See the Appendix 6.3 for details of the VQA data construction.

2.3 Progressive Training via SFT and Cascaded RL

To cultivate the hybrid-thinking capabilities of *DriveAgent-RI*, we devise a progressive training strategy composed of an initial Supervised Fine-Tuning (SFT) stage and a subsequent two-stage Cascaded RL phase shown in Fig. 3. This overall strategy follows a “foundation building \rightarrow mode strengthening \rightarrow intelligent selection” paradigm.

2.3.1 Stage 1: Dual-Mode Supervised Fine-Tuning

We begin by cold-starting the model using SFT to endow it with a foundational understanding of the format and semantic boundaries of both thinking modes. To this end, we construct a high-quality dataset via a three-stage automated pipeline. The pipeline first partitions raw data into a tool-unnecessary set D_{text} and a tool-necessary set D_{tool} . D_{text} comprises simple scenarios where Qwen2.5-VL-3B already achieves high accuracy without tools, indicating no need for active perception. Conversely, D_{tool} includes complex cases where the powerful Qwen2.5-VL-72B shows a performance gain only when using tools, establishing a criterion for tool necessity. Next, Qwen2.5-VL-72B generates mode-specific CoT annotations. To ensure data quality, these annotations undergo a rigorous validation and filtering process: a separate judge model scores the reasoning coherence, and samples falling below a quality threshold are automatically regenerated. Finally, the data is passed through rule-based cleaning to create a balanced, high-quality dataset for SFT. A complete description of this pipeline is provided in Appendix 6.4.

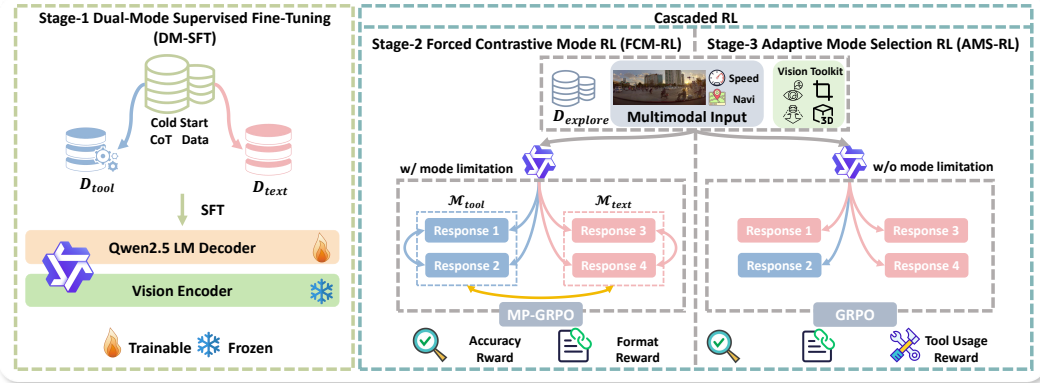


Figure 3: The progressive three-stage training strategy for *DriveAgent-RL*. The process begins with (1) DM-SFT to establish a foundational understanding of both thinking modes. This is followed by a core Cascaded RL phase, where (2) FCM-RL strengthens each mode independently, and (3) AMS-RL trains the agent to adaptively select the optimal mode.

2.3.2 Stage 2: Forced Contrastive Mode Reinforcement Learning

The first stage of our Cascaded RL phase aims to deepen the agent’s independent performance in each mode. We employ RL to unlock the model’s potential, ensuring it does not develop a bias against an initially weaker mode, which is critical for the subsequent adaptive selection stage.

To this end, we propose Mode-Partitioned GRPO (MP-GRPO), a variant of the GRPO algorithm [23, 24], which has proven effective in multimodal reasoning and autonomous driving [14, 25, 26, 27]. As illustrated in Fig. 3, the core mechanism of MP-GRPO is to enforce balanced exploration across both thinking modes. For each input q from D_{explore} , we compel the agent to generate two mode-specific sets of $G/2$ responses by forcing the corresponding mode token (`<think_text>` or `<think_tool>`). This creates a full group of G responses:

$$\mathcal{O}(q) = \{o_i^{\text{text}}\}_{i=1}^{G/2} \cup \{o_j^{\text{tool}}\}_{j=1}^{G/2},$$

where each individual response, denoted by o , is sampled from the old policy $\pi_{\theta_{\text{old}}}$. Crucially, all G responses are then aggregated into this unified set $\mathcal{O}(q)$ for reward normalization and advantage calculation. This design creates a **multi-dimensional contrastive learning signal**: it facilitates not only **intra-mode** comparison between different response trajectories but also **inter-mode** comparison. This multi-faceted contrast allows the agent to simultaneously enhance its specific capabilities in both modes and gain an initial understanding of the suitability of each mode for different scenarios, laying a critical foundation for the final stage of adaptive selection.

Reward Design. The agent’s learning is guided by an outcome-driven reward function that evaluates the entire reasoning trajectory. This reward is a composite of two key components: an accuracy reward (R_{acc}) and a format consistency reward (R_{fmt}), formulated as follows:

$$R = R_{\text{acc}} + R_{\text{fmt}},$$

where the accuracy reward R_{acc} is a weighted Levenshtein distance against the ground-truth sequence, with position-action weights to counteract action imbalance (see Appendix 6.5 for details). The format consistency reward R_{fmt} penalizes structural errors and incorrect mode usage, such as invoking tools in the $\mathcal{M}_{\text{text}}$ mode.

2.3.3 Stage 3: Adaptive Mode Selection Reinforcement Learning

The final stage of Cascaded RL cultivates true hybrid thinking by training the agent to intelligently select the optimal thinking mode. Using the native GRPO algorithm [23, 24], the agent learns to generate the initial mode-selection token (`<think_text>` or `<think_tool>`) itself and commit to the corresponding reasoning path.

Reward Design. To guide this learning process, the reward function is augmented with a conditional tool-usage reward, R_{tool} , which encourages the effective and judicious use of tools only when the

$\mathcal{M}_{\text{tool}}$ mode is chosen. The total reward is defined as:

$$R = R_{\text{acc}} + R_{\text{fmt}} + \mathbb{I}(\text{mode} = \mathcal{M}_{\text{tool}}) \cdot R_{\text{tool}},$$

where the definitions of R_{acc} and R_{fmt} remain consistent with Stage 2. The core of R_{tool} is a **contrastive mechanism** that promotes impactful tool use. Within each group of G generated responses, we establish a baseline by calculating the average accuracy of all text-only trajectories (\bar{Acc}_{text}). A tool-based trajectory is rewarded only if its own accuracy (R_{acc}) surpasses this baseline by a margin, i.e., $R_{\text{tool}} \propto (R_{\text{acc}} - \bar{Acc}_{\text{text}} - \text{margin})$. This design explicitly penalizes superfluous tool calls, incentivizing the agent to invoke active perception only when it provides a clear performance advantage over pure text-based reasoning. A detailed formulation is provided in the Appendix 6.5.

3 Experiments

3.1 Setup

3.1.1 Dataset

Automated Label Generation for Meta-actions. We produce labels for meta-action sequences with a rule-first, VLM-corrected pipeline. Starting from vehicle trajectory points, we use a 3-second sliding window to map each segment to a predefined vocabulary of speed and trajectory actions. This yields a four-step discrete meta-action sequence for the next 8 seconds at 2-second intervals. To correct a small number of ambiguous or boundary cases, we then feed the resulting sequence and its BEV-map visualization into GPT-4.1 for refinement. Full rules and prompt details are in the Appendix 6.7.

Training Data. All training data are drawn from our Drive-Internal dataset, which comprises 35K video clips specifically targeting long-tail and complex scenarios. This dataset features over 40 distinct driving situations, including challenging events like road works and animal crossings. To leverage its rich diversity, one or two key frames are sampled from each clip, focusing on the moments surrounding critical events. For Stage 1 (DM-SFT), we generate 4K high-quality CoT data using the pipeline from Sec. 2.3.1, splitting it evenly into the tool-necessary set D_{tool} and the tool-unnecessary set D_{text} (2K each). For the Cascaded RL phase, we construct an exploratory set D_{explore} by sampling 15K instances from the data not assigned to D_{tool} or D_{text} , ensuring the sampling maintains a balanced distribution of actions at each timestep in the sequence.

Test Data. We randomly sample 1.5K instances from Drive-Internal as the in-distribution test set $\text{Drive-Internal}_{\text{test}}$. To assess generalization, we also sample 2K instances from the nuScenes validation set as $\text{nuScenes}_{\text{test}}$ for cross-dataset testing. All nuScenes samples are taken from the middle of each clip to ensure sufficient history and future trajectories. Meta-action labels on nuScenes are generated by the same pipeline.

3.1.2 Evaluation Metrics

Accuracy (Acc). We evaluate planning precision using First-Frame and Sequence Average Joint Accuracy. A prediction is considered correct only if the composite meta-action (both speed and trajectory) exactly matches the ground truth. To encourage safer behavior, we also employ a Relaxed Speed Matching mechanism, awarding partial scores (0.5 and 0.2) for predictions that are one and two levels safer than the ground truth, respectively.

Mode Selection Accuracy (MSA). To quantify *DriveAgent-RI*'s adaptive mode selection, we introduce the Mode Selection Accuracy (MSA), inspired by (author?) [28]. It measures the alignment between the agent's adaptively chosen mode m_{adaptive} and the optimal mode m_i^* . The optimal mode m_i^* is defined as whichever mode ($\mathcal{M}_{\text{tool}}$ or $\mathcal{M}_{\text{text}}$) achieves higher accuracy for a given sample q_i . MSA is then calculated as:

$$MSA = \frac{1}{N} \sum_{i=1}^N \mathbb{I}(m_{\text{adaptive}}(q_i) = m_i^*)$$

Table 1: Main results on the Drive-Internal_{test} and nuScenes_{test}. All models are evaluated using one-shot prompting under two conditions: without tools and with access to the visual toolkit. To ensure a consistent, structured reasoning format, closed-source models were queried via their official APIs in a “no-thinking” mode. Parentheses show the absolute gain from using tools.

Model	Drive-Internal _{test}				nuScenes _{test}			
	First-Frame Joint Acc. (%)		Seq. Avg. Joint Acc. (%)		First-Frame Joint Acc. (%)		Seq. Avg. Joint Acc. (%)	
	w/o Tools	w/ Tools	w/o Tools	w/ Tools	w/o Tools	w/ Tools	w/o Tools	w/ Tools
Human	49.59		49.29		50.48		48.24	
Qwen2.5-VL-3B	24.06	23.64 (-0.42)	24.98	22.63 (-2.35)	30.18	28.17 (-2.01)	23.48	21.58 (-1.90)
Qwen2.5-VL-7B	27.58	24.01 (-3.57)	29.84	24.98 (-4.86)	33.11	32.84 (-0.27)	27.60	28.82 (+1.22)
Qwen2.5-VL-72B	32.76	32.97 (+0.21)	38.80	39.61 (+0.81)	43.26	43.87 (+0.61)	39.13	40.47 (+1.34)
Doubao-Seed-1.6	34.92	38.98 (+4.06)	40.22	41.37 (+1.15)	45.63	46.29 (+0.66)	41.91	43.10 (+1.19)
Gemini-2.5-Flash	41.83	43.38 (+1.55)	42.14	43.42 (+1.28)	45.46	46.60 (+1.14)	42.69	44.07 (+1.38)
GPT-4.1	39.99	43.18 (+3.19)	42.14	43.43 (+1.29)	46.84	48.25 (+1.41)	43.63	44.72 (+1.09)
GPT-5	56.30	56.48 (+0.18)	47.19	47.97 (+0.78)	48.75	49.11 (+0.36)	44.85	45.14 (+0.29)
DriveAgent-R1	45.27	<u>51.34</u> (+6.07)	43.29	<u>45.42</u> (+2.13)	52.58	52.96 (+0.38)	44.43	47.10 (+2.67)

3.1.3 Implementation Details

All training is conducted on 8 H20 GPUs. For all multimodal inputs in our experiments, the maximum number of pixels per image is set to 259,200. Unless specified, only the front-view camera image serves as the default visual input. During the Cascaded RL phase, we set the sampling temperature to 1.0, limit the maximum number of tool calls to 3, and group size to 4 per sample. For all evaluations, the sampling temperature is set to 0.7.

3.2 Main results

To comprehensively evaluate *DriveAgent-R1*, we benchmark it against a suite of state-of-the-art closed-source VLMs, the open-source Qwen2.5-VL series, and a human performance baseline on both the Drive-Internal_{test} and nuScenes_{test}. More details are shown in Appendix 6.8. The main results are summarized in Table 1, leading to two key observations.

DriveAgent-R1 achieves performance comparable to GPT-5 and human drivers with only 3B parameters. Despite its 3B parameter size, *DriveAgent-R1* shows remarkable performance and the most effective tool use, achieving a +6.0% accuracy gain on Drive-Internal_{test}. Its performance is competitive with both GPT-5 and human drivers. Notably, on the nuScenes_{test}, *DriveAgent-R1* surpasses GPT-5 in sequence accuracy (47.10% vs. 45.14%) and approaches human-level proficiency.

Visual tool is a double-edged sword. While VLMs like GPT-4.1 and Gemini-2.5-Flash improved with tool access, the Qwen2.5-VL-3B and -7B models showed consistent performance degradation. This indicates that effective tool use is a non-trivial skill, requiring either a high level of base model capability or targeted, specialized training to master.

Table 2: **Analysis of Foundational Capabilities.** Overall scores on domain-specific and 8 general VLM benchmarks. Numbers in blue denote the improvement over Qwen2.5-VL-3B. Detail results are in Appendix 6.9.1.

Model	DriveAlign-VQA _{test}	General Benchmarks
Qwen2.5-VL-3B	72.9	64.4
Qwen2.5-VL-7B	77.0	68.9
DriveAlign-3B	84.6 (+11.7)	66.4 (+2.0)

Table 3: **Impact of Domain Alignment on High-Level Behavioral Planning Task.** We report sequence accuracy on Drive-Internal_{test}. The relative performance drop (%) upon removing images is shown in parentheses.

Base Model	Model	Seq. Avg. Joint Acc. (%)	
		w/ image	w/o image (rel. drop)
Qwen2.5-VL-3B	DriveAgent-R1-Variant	43.56	38.79 (-11.0%)
DriveAlign-3B	DriveAgent-R1	45.42	38.24 (-15.8%)

3.3 Ablation on Domain Alignment

To validate our domain alignment strategy, we analyze its impact on both the base model’s capabilities and the downstream high-level behavioral planning task.

Domain Alignment Enhances Driving-Specific and General Capabilities. As shown in Table 2, domain alignment significantly boosts performance on our driving-specific VQA benchmark (+11.7) and also improves scores across a suite of general VLM benchmarks (+2.0). This confirms our strategy successfully injects domain knowledge while strengthening general capabilities.

Domain Alignment Boosts Planning Performance and Mitigates Visual Neglect. As shown in Table 3, the agent built on our aligned model achieves higher accuracy (+1.86 Sequence Avg-Joint Acc). Crucially, its performance drops more significantly when images are removed (-15.8% vs. -11.0%), confirming its gains are grounded in visual evidence rather than textual shortcuts, thereby mitigating the visual neglect problem.

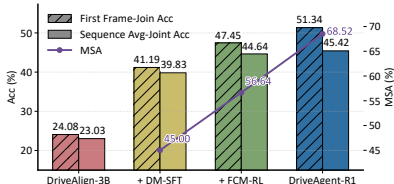


Figure 4: **Progressive training gains on Drive-Internal_{test}.** Accuracy in $\mathcal{M}_{\text{adaptive}}$ mode and MSA improve with each training stage.

Table 4: **Ablation on the progressive training strategy on the Drive-Internal_{test}.** We evaluate different combinations of our three training stages. To ensure fair comparison, we also test variants where a single RL stage is trained for two epochs, matching the total RL epochs of *DriveAgent-R1*.

Variant	Training Stage			Seq. Avg. Joint Acc. (%)			MSA (%)
	DM-SFT	FCM-RL	AMS-RL	$\mathcal{M}_{\text{tool}}$	$\mathcal{M}_{\text{text}}$	$\mathcal{M}_{\text{adaptive}}$	
Variant-1 (SFT Only)	1 epoch	-	-	42.02	40.65	40.88	45.00
Variant-2 (+FCM)	1 epoch	1 epoch	-	44.30	42.20	44.64	56.64
Variant-3 (+FCM x2)	1 epoch	2 epochs	-	43.89	42.81	44.91	57.32
Variant-4 (+AMS)	1 epoch	-	1 epoch	43.78	41.64	43.43	57.55
Variant-5 (+AMS x2)	1 epoch	-	2 epochs	44.76	42.56	44.13	61.61
DriveAgent-R1 (FCM→AMS)	1 epoch	1 epoch	1 epoch	44.97	43.29	45.42	68.52

3.4 Ablation on Progressive Training Strategy

To validate our progressive training strategy, we ablate different stage combinations in forced-text ($\mathcal{M}_{\text{text}}$), forced-tool ($\mathcal{M}_{\text{tool}}$), and adaptive-selection ($\mathcal{M}_{\text{adaptive}}$) modes on both the Drive-Internal_{test} and nuScenes_{test} datasets to confirm the method’s effectiveness (full nuScenes_{test} results are in the Appendix 6.9.2). Our analysis yields two key findings.

Progressive Training Yields Stable Performance Gains. As illustrated in Fig. 4, our strategy achieves consistent performance improvements, resulting in a steady increase in both accuracy and MSA.

The Cascaded RL Strategy Surpasses Single-Strategy Stacking due to Functional Complementarity. Table 4 reveals that our cascaded RL strategy is synergistic, outperforming single-strategy stacking with the same total training epochs (Variant-3/5). This superiority stems from the complementary roles of its two stages: FCM-RL sharpens execution proficiency (achieving higher forced-mode accuracies of 44.30% vs. 43.78% in $\mathcal{M}_{\text{tool}}$ and 42.20% vs. 41.64% in $\mathcal{M}_{\text{text}}$, while AMS-RL hones selection intelligence (yielding a higher MSA of 57.55% vs. 56.64%). Our cascaded approach successfully integrates these distinct strengths for superior overall performance.

Table 5: **Ablation on Active vs. Passive Perception.** We compare *DriveAgent-R1* with passive baselines on Drive-Internal_{test}. Relative drop (%) without images in parentheses.

Model	Seq. Avg. Joint Acc. (%)	
	w/ image	w/o image (rel. drop)
Passive-FV	42.70	39.64 (-7.2%)
Passive-SV	43.10	39.01 (-9.5%)
DriveAgent-R1 (Retrieve View Only)	44.39	38.78 (-12.6%)
DriveAgent-R1 (Full Toolkit)	45.42	38.24 (-15.8%)

Table 6: **Performance and Efficiency Analysis.** We compare inference latency and average output tokens for different perception and reasoning strategies.

Model/Mode	Latency (s)	Avg. Token
Passive-SV	8.50	210.77
DriveAgent-R1 ($\mathcal{M}_{\text{tool}}$)	7.91	314.45
DriveAgent-R1 ($\mathcal{M}_{\text{adaptive}}$)	6.74	265.57

3.5 Ablation on Active versus Passive Perception

To isolate the benefits of active perception, we compare *DriveAgent-R1* against two passive perception baselines: Passive-FV (front-view) and Passive-SV (surrounding views), all of which were trained with the same SFT and RL pipeline for a fair comparison. For a controlled comparison against Passive-SV, we evaluate a restricted variant, *DriveAgent-R1 (Retrieve View Only)*, which is limited to using only the “Retrieve View” tool. As shown in Table 5, our findings are twofold.

Active Selection is Superior to Passive Input. Active perception, as demonstrated by *DriveAgent-RI* (Retrieve View Only), shows a dual advantage. First, it overcomes information deficits (outperforming Passive-FV by +1.69 points). Second, it mitigates the redundancy of multiple fixed views. Despite sharing an identical information ceiling (the same pool of six views), *DriveAgent-RI* outperforms the Passive-SV by +1.29 points. This confirms that actively retrieving task-relevant information on demand is more effective than passively processing a fixed set of inputs.

Active Perception Deepens Visual Reliance. A clear trend emerges: the more active and capable the agent’s perception, the more its performance drops when visual inputs are removed. This confirms our framework successfully fosters a genuine, vision-driven decision-making process, steering the model away from textual shortcuts. This heightened dependence on vision, however, also underscores the criticality of correctly interpreting the acquired evidence. In complex scenarios, misinterpreting new visual information can lead to errors, a challenge we explore in Appendix 6.11.

3.6 Efficiency Analysis

To assess the computational efficiency of our framework, we evaluate inference latency and average output token length. Latency is measured on a single H20 GPU with a batch size of 1 using the vLLM [29] inference framework, averaged over 100 samples and repeated across 5 runs. The results, summarized in Table 6, highlight two key advantages of our design.

Active Perception is More Efficient than Passive Input. By selectively retrieving visual data only when needed, *DriveAgent-RI* avoids the computational overhead of processing the redundant images required by Passive-SV. This targeted approach reduces inference latency by over 20%.

Hybrid Thinking Balances Performance and Cost. The advantage of hybrid thinking is clear when comparing the ($\mathcal{M}_{\text{adaptive}}$ and $\mathcal{M}_{\text{tool}}$ modes. *DriveAgent-RI* under $\mathcal{M}_{\text{adaptive}}$ reduces both inference latency (from 7.91s to 6.74s) and output tokens (from 314.45 to 265.57).

4 Related Work

VLMs for Autonomous Driving. Recent advancements have seen Vision-Language Models (VLMs) applied to autonomous driving, unifying perception, reasoning, and planning [2, 1, 30]. Research has primarily followed two paths: enhancing structured scene understanding [2, 31, 32, 33] and translating reasoning into actionable behaviors, from high-level decisions to low-level motion planning [14, 15, 1]. However, existing VLM-based planners predominantly operate under a passive perception paradigm, reasoning over a fixed set of inputs. *DriveAgent-RI* breaks from this by introducing an active perception framework, where the agent proactively invokes a visual toolkit to ground its decisions in visual evidence.

Multimodal Reasoning with Chain-of-Thought. Chain-of-Thought (CoT) has significantly improved the reasoning capabilities of LLMs [34, 35, 36] and has been extended to the multimodal domain (M-CoT) [9, 37, 38, 39, 25]. The evolution of M-CoT has progressed from Text-based methods, which reason over static textual descriptions [9, 40, 41], to more dynamic, interleaved approaches. Among these, Tool-based M-CoT is a promising direction, enabling models to actively seek new information during reasoning [31, 11, 13, 26, 27]. Our work advances this frontier by introducing a novel hybrid-thinking paradigm that adaptively integrates efficient Text-based M-CoT with robust Tool-based M-CoT, allowing the agent to modulate its reasoning depth according to the scene’s complexity.

5 Conclusion and Limitations

We introduced *DriveAgent-RI*, an autonomous driving agent that pioneers active perception and hybrid thinking for high-level behavioral planning. Our 3B model achieves performance competitive with top-tier systems like GPT-5 and human drivers while being deployment-friendly. However, a key limitation is the agent’s over-reliance on new visual evidence from its tools, as detailed in our failure case analysis (Appendix 6.11). Future work will directly address this challenge through two complementary directions: (1) strengthening the agent’s foundational understanding of complex road topologies and traffic rules, and (2) cultivating a more nuanced reasoning process capable of resolving informational conflicts.

References

- [1] Xiaoyu Tian, Junru Gu, Bailin Li, Yicheng Liu, Zhiyong Zhao, Yang Wang, Kun Zhan, Peng Jia, Xianpeng Lang, and Hang Zhao. Drivevlm: The convergence of autonomous driving and large vision-language models. *arXiv preprint arXiv:2402.12289*, 2024.
- [2] Chonghao Sima, Katrin Renz, Kashyap Chitta, Li Chen, Hanxue Zhang, Chengen Xie, Jens Beißwenger, Ping Luo, Andreas Geiger, and Hongyang Li. Drivelm: Driving with graph visual question answering. In *ECCV*, 2024.
- [3] Zhenhua Xu, Yujia Zhang, Enze Xie, Zhen Zhao, Yong Guo, Kwan-Yee K. Wong, Zhenguo Li, and Hengshuang Zhao. Drivegpt4: Interpretable end-to-end autonomous driving via large language model. *IEEE Robotics and Automation Letters*, 2024.
- [4] Yihan Hu, Jiazhi Yang, Li Chen, Keyu Li, Chonghao Sima, Xizhou Zhu, Siqi Chai, Senyao Du, Tianwei Lin, Wenhai Wang, et al. Planning-oriented autonomous driving. In *CVPR*, 2023.
- [5] Bo Jiang, Shaoyu Chen, Qing Xu, Bencheng Liao, Jiajie Chen, Helong Zhou, Qian Zhang, Wenyu Liu, Chang Huang, and Xinggang Wang. Vad: Vectorized scene representation for efficient autonomous driving. In *ICCV*, 2023.
- [6] Yuping Wang, Shuo Xing, Cui Can, Renjie Li, Hongyuan Hua, Kexin Tian, Zhaobin Mo, Xiangbo Gao, Keshu Wu, Sulong Zhou, et al. Generative ai for autonomous driving: Frontiers and opportunities. *arXiv preprint arXiv:2505.08854*, 2025.
- [7] Letian Wang, Yeping Hu, Liting Sun, Wei Zhan, Masayoshi Tomizuka, and Changliu Liu. Transferable and adaptable driving behavior prediction. *arXiv preprint arXiv:2202.05140*, 2022.
- [8] Pranjal Paul, Anant Garg, Tushar Choudhary, Arun Kumar Singh, and K Madhava Krishna. Lego-drive: Language-enhanced goal-oriented closed-loop end-to-end autonomous driving. In *IROS*, 2024.
- [9] Guowei Xu, Peng Jin, Ziang Wu, Hao Li, Yibing Song, Lichao Sun, and Li Yuan. Llava-cot: Let vision language models reason step-by-step. *ICCV*, 2025.
- [10] Chengzu Li, Wenshan Wu, Huanyu Zhang, Yan Xia, Shaoguang Mao, Li Dong, Ivan Vulić, and Furu Wei. Imagine while reasoning in space: Multimodal visualization-of-thought. *arXiv preprint arXiv:2501.07542*, 2025.
- [11] OpenAI. Introducing O3 and O4 mini. <https://openai.com/index/introducing-o3-and-o4-mini/>, 2025. Accessed: 2025-07-24.
- [12] Zihui Cheng, Qiguang Chen, Xiao Xu, Jiaqi Wang, Weiyun Wang, Hao Fei, Yidong Wang, Alex Jinpeng Wang, Zhi Chen, Wanxiang Che, et al. Visual thoughts: A unified perspective of understanding multimodal chain-of-thought. *arXiv preprint arXiv:2505.15510*, 2025.
- [13] Yushi Hu, Weijia Shi, Xingyu Fu, Dan Roth, Mari Ostendorf, Luke Zettlemoyer, Noah A Smith, and Ranjay Krishna. Visual sketchpad: Sketching as a visual chain of thought for multimodal language models. In *NeurIPS*, 2024.
- [14] Bo Jiang, Shaoyu Chen, Qian Zhang, Wenyu Liu, and Xinggang Wang. Alphadrive: Unleashing the power of vlms in autonomous driving via reinforcement learning and reasoning. *arXiv preprint arXiv:2503.07608*, 2025.
- [15] Yue Li, Meng Tian, Dechang Zhu, Jiangtong Zhu, Zhenyu Lin, Zhiwei Xiong, and Xinhai Zhao. Drive-r1: Bridging reasoning and planning in vlms for autonomous driving with reinforcement learning, 2025.
- [16] Zhijie Qiao, Haowei Li, Zhong Cao, and Henry X Liu. Lightemma: Lightweight end-to-end multimodal model for autonomous driving. *arXiv preprint arXiv:2505.00284*, 2025.
- [17] Yihan Hu, Jiazhi Yang, Li Chen, Keyu Li, Chonghao Sima, Xizhou Zhu, Siqi Chai, Senyao Du, Tianwei Lin, Wenhai Wang, Lewei Lu, Xiaosong Jia, Qiang Liu, Jifeng Dai, Yu Qiao, and Hongyang Li. Planning-oriented autonomous driving. In *CVPR*, 2023.

- [18] Wenchao Sun, Xuewu Lin, Yining Shi, Chuang Zhang, Haoran Wu, and Sifa Zheng. Sparsedrive: End-to-end autonomous driving via sparse scene representation. In *ICRA*, 2025.
- [19] OpenAI. GPT-5. Technical report, OpenAI, 2025. Accessed: 2025-9-22.
- [20] Xuesong Chen, Linjiang Huang, Tao Ma, Rongyao Fang, Shaoshuai Shi, and Hongsheng Li. Solve: Synergy of language-vision and end-to-end networks for autonomous driving. In *CVPR*, 2025.
- [21] Shihao Wang, Zhiding Yu, Xiaohui Jiang, Shiyi Lan, Min Shi, Nadine Chang, Jan Kautz, Ying Li, and Jose M. Alvarez. OmniDrive: A holistic vision-language dataset for autonomous driving with counterfactual reasoning. In *CVPR*, 2025.
- [22] Shuai Bai, Keqin Chen, Xuejing Liu, Jialin Wang, Wenbin Ge, Sibao Song, Kai Dang, Peng Wang, Shijie Wang, Jun Tang, Humen Zhong, Yuanzhi Zhu, Mingkun Yang, Zhaohai Li, Jianqiang Wan, Pengfei Wang, Wei Ding, Zheren Fu, Yiheng Xu, Jiabo Ye, Xi Zhang, Tianbao Xie, Zesen Cheng, Hang Zhang, Zhibo Yang, Haiyang Xu, and Junyang Lin. Qwen2.5-vl technical report. *arXiv preprint arXiv:2502.13923*, 2025.
- [23] Zhihong Shao, Peiyi Wang, Qihao Zhu, Runxin Xu, Junxiao Song, Xiao Bi, Haowei Zhang, Mingchuan Zhang, YK Li, Yang Wu, et al. Deepseekmath: Pushing the limits of mathematical reasoning in open language models. *CoRR*, 2024.
- [24] Daya Guo, Dejian Yang, Haowei Zhang, Junxiao Song, Ruoyu Zhang, Runxin Xu, Qihao Zhu, Shirong Ma, Peiyi Wang, Xiao Bi, et al. Deepseek-r1: Incentivizing reasoning capability in llms via reinforcement learning. *arXiv preprint arXiv:2501.12948*, 2025.
- [25] Ziyu Liu, Zeyi Sun, Yuhang Zang, Xiaoyi Dong, Yuhang Cao, Haodong Duan, Dahua Lin, and Jiaqi Wang. Visual-rft: Visual reinforcement fine-tuning. *arXiv preprint arXiv:2503.01785*, 2025.
- [26] Alex Su, Haozhe Wang, Weiming Ren, Fangzhen Lin, and Wenhui Chen. Pixel reasoner: Incentivizing pixel-space reasoning with curiosity-driven reinforcement learning. *arXiv preprint arXiv:2505.15966*, 2025.
- [27] Ziwei Zheng, Michael Yang, Jack Hong, Chenxiao Zhao, Guohai Xu, Le Yang, Chao Shen, and Xing Yu. Deepeyes: Incentivizing "thinking with images" via reinforcement learning. *arXiv preprint arXiv:2505.14362*, 2025.
- [28] Lingjie Jiang, Xun Wu, Shaohan Huang, Qingxiu Dong, Zewen Chi, Li Dong, Xingxing Zhang, Tengchao Lv, Lei Cui, and Furu Wei. Think only when you need with large hybrid-reasoning models, 2025.
- [29] Woosuk Kwon, Zhuohan Li, Siyuan Zhuang, Ying Sheng, Lianmin Zheng, Cody Hao Yu, Joseph E. Gonzalez, Hao Zhang, and Ion Stoica. Efficient memory management for large language model serving with pagedattention. In *SOSP*, 2023.
- [30] Jiageng Mao, Yuxi Qian, Junjie Ye, Hang Zhao, and Yue Wang. Gpt-driver: Learning to drive with gpt. *arXiv preprint arXiv:2310.01415*, 2023.
- [31] Kangan Qian, Sicong Jiang, Yang Zhong, Ziang Luo, Zilin Huang, Tianze Zhu, Kun Jiang, Mengmeng Yang, Zheng Fu, Jinyu Miao, et al. Agentthink: A unified framework for tool-augmented chain-of-thought reasoning in vision-language models for autonomous driving. *arXiv preprint arXiv:2505.15298*, 2025.
- [32] Ming Nie, Renyuan Peng, Chunwei Wang, Xinyue Cai, Jianhua Han, Hang Xu, and Li Zhang. Reason2drive: Towards interpretable and chain-based reasoning for autonomous driving. In *ECCV*, 2024.
- [33] Hao Shao, Yuxuan Hu, Letian Wang, Guanglu Song, Steven L Waslander, Yu Liu, and Hongsheng Li. Lmdrive: Closed-loop end-to-end driving with large language models. In *CVPR*, 2024.

- [34] Jason Wei, Xuezhi Wang, Dale Schuurmans, Maarten Bosma, Fei Xia, Ed Chi, Quoc V Le, Denny Zhou, et al. Chain-of-thought prompting elicits reasoning in large language models. *NeurIPS*, 2022.
- [35] Zheng Chu, Jingchang Chen, Qianglong Chen, Weijiang Yu, Tao He, Haotian Wang, Weihua Peng, Ming Liu, Bing Qin, and Ting Liu. Navigate through enigmatic labyrinth a survey of chain of thought reasoning: Advances, frontiers and future. *arXiv preprint arXiv:2309.15402*, 2023.
- [36] Xuezhi Wang and Denny Zhou. Chain-of-thought reasoning without prompting. *NeurIPS*, 2024.
- [37] Liqi He, Zuchao Li, Xiantao Cai, and Ping Wang. Multi-modal latent space learning for chain-of-thought reasoning in language models. In *AAAI*, 2024.
- [38] Lei Wang, Yi Hu, Jiabang He, Xing Xu, Ning Liu, Hui Liu, and Heng Tao Shen. T-sciq: Teaching multimodal chain-of-thought reasoning via large language model signals for science question answering. In *AAAI*, 2024.
- [39] Debjyoti Mondal, Suraj Modi, Subhadarshi Panda, Rituraj Singh, and Godawari Sudhakar Rao. Kam-cot: Knowledge augmented multimodal chain-of-thoughts reasoning. In *AAAI*, 2024.
- [40] Kesen Zhao, Beier Zhu, Qianru Sun, and Hanwang Zhang. Unsupervised visual chain-of-thought reasoning via preference optimization. *arXiv preprint arXiv:2504.18397*, 2025.
- [41] Hongyu Li, Jinyu Chen, Ziyu Wei, Shaofei Huang, Tianrui Hui, Jialin Gao, Xiaoming Wei, and Si Liu. Llava-st: A multimodal large language model for fine-grained spatial-temporal understanding. In *CVPR*, 2025.
- [42] Lihe Yang, Bingyi Kang, Zilong Huang, Zhen Zhao, Xiaogang Xu, Jiashi Feng, and Hengshuang Zhao. Depth anything v2. *NeurIPS*, 2024.
- [43] Hanxue Zhang, Haoran Jiang, Qingsong Yao, Yanan Sun, Renrui Zhang, Hao Zhao, Hongyang Li, Hongzi Zhu, and Zetong Yang. Detect anything 3d in the wild. In *ICCV*, 2025.
- [44] Lin Chen, Jinsong Li, Xiaoyi Dong, Pan Zhang, Yuhang Zang, Zehui Chen, Haodong Duan, Jiaqi Wang, Yu Qiao, Dahua Lin, and Feng Zhao. Are we on the right way for evaluating large vision-language models? In *NeurIPS*, 2024.
- [45] Weihao Yu, Zhengyuan Yang, Linjie Li, Jianfeng Wang, Kevin Lin, Zicheng Liu, Xinchao Wang, and Lijuan Wang. Mm-vet: Evaluating large multimodal models for integrated capabilities. In *ICML*, 2024.
- [46] Yuan Liu, Haodong Duan, Yuanhan Zhang, Bo Li, Songyang Zhang, Wangbo Zhao, Yike Yuan, Jiaqi Wang, Conghui He, Ziwei Liu, et al. Mmbench: Is your multi-modal model an all-around player? In *ECCV*, 2024.
- [47] Yi-Fan Zhang, Huanyu Zhang, Haochen Tian, Chaoyou Fu, Shuangqing Zhang, Junfei Wu, Feng Li, Kun Wang, Qingsong Wen, Zhang Zhang, et al. Mme-realworld: Could your multimodal llm challenge high-resolution real-world scenarios that are difficult for humans? In *ICLR*, 2024.
- [48] Yuliang Liu, Zhang Li, Mingxin Huang, Biao Yang, Wenwen Yu, Chunyuan Li, Xu-Cheng Yin, Cheng-Lin Liu, Lianwen Jin, and Xiang Bai. Ocrbench: on the hidden mystery of ocr in large multimodal models. *Science China Information Sciences*, 2024.
- [49] Xiang Yue, Yuansheng Ni, Kai Zhang, Tianyu Zheng, Ruoqi Liu, Ge Zhang, Samuel Stevens, Dongfu Jiang, Weiming Ren, Yuxuan Sun, Cong Wei, Botao Yu, Ruibin Yuan, Renliang Sun, Ming Yin, Boyuan Zheng, Zhenzhu Yang, Yibo Liu, Wenhao Huang, Huan Sun, Yu Su, and Wenhua Chen. Mmmu: A massive multi-discipline multimodal understanding and reasoning benchmark for expert agi. In *CVPR*, 2024.
- [50] Aniruddha Kembhavi, Mike Salvato, Eric Kolve, Minjoon Seo, Hannaneh Hajishirzi, and Ali Farhadi. A diagram is worth a dozen images. In *ECCV*, 2016.
- [51] Haodong Duan, Junming Yang, Yuxuan Qiao, Xinyu Fang, Lin Chen, Yuan Liu, Xiaoyi Dong, Yuhang Zang, Pan Zhang, Jiaqi Wang, et al. Vlmevalkit: An open-source toolkit for evaluating large multi-modality models. In *ACM MM*, 2024.

6 Appendix

6.1 Usage of LLM

Large Language Models were utilized as a writing aid in the preparation of this manuscript. Their use was strictly limited to improving the clarity and readability of the text through sentence polishing and grammar correction. Additionally, we consulted LLMs for brainstorming potential names for concepts and components, such as $\mathcal{M}_{\text{adaptive}}$, DriveAlign-3B, and Drive-Internal. The core methodology, experimental results, and scientific insights presented in this paper are the original work of the authors.

6.2 Vision Toolkit: Detailed Descriptions and Call Formats

Retrieve View. This tool allows the agent to request the image from any specific viewpoint. Its design is motivated by human drivers who consciously check specific mirrors or windows to get a clear view of the road conditions before critical maneuvers like lane changes or turns. More importantly, this tool incorporates a Historical Memory Pool, which caches images from all viewpoints over the past 5 seconds, sampled at 1Hz. This enables the model to intelligently look back at historical frames to assess changes in traffic light status or the movement trends of dynamic objects, thus avoiding the high computational cost and latency associated with processing redundant information from full video sequences.

```
<tool_call>
  <tool_name>Retrieve View</tool_name>
  <params>{"frame_index": "-1s", "view_index": "front_left"}</params>
</tool_call>
```

Listing 1: Call Format of Retrieve View

RoI Inspection. This tool empowers the agent with a “zoom-in” capability for meticulous examination of critical areas. Based on a selected view, the agent can request to retrieve a higher-resolution version of the image and then crop and magnify a specific Region of Interest (RoI) by providing the absolute pixel coordinates of its bounding box. This is not merely a passive utility; it is a direct manifestation of the model’s Inherent Localization Ability. This allows for fine-grained analysis and focused viewing of any region the agent deems important, which is vital for confirming details such as the status of distant traffic lights or the text on traffic signs.

```
<tool_call>
  <tool_name>RoI Inspection</tool_name>
  <params>{"view_index": "front_left", "bbox": [x_min, y_min, x_max,
    y_max], "description": "the traffic lights"}</params>
</tool_call>
```

Listing 2: Call Format of RoI Inspection

Depth Estimation. Accurately perceiving the 3D spatial relationship between the ego-vehicle and other traffic participants (e.g., vehicles, pedestrians) is fundamental to safe driving. This tool leverages the state-of-the-art monocular depth estimation algorithm, Depth Anything V2 [42], to generate a depth map for a specified view. The resulting depth map provides rich geometric information, enabling the model to intuitively grasp the relative distances and spatial layout of objects, as well as the overall road structure, which is crucial for path planning and obstacle avoidance.

```
<tool_call>
  <tool_name>Depth Estimation</tool_name>
  <params>{"view_index": "front"}</params>
</tool_call>
```

Listing 3: Call Format of Depth Estimation

3D Object Detection. To comprehensively understand the dynamic environment, the agent must identify key objects and ascertain their precise 3D spatial information (position, size, and orientation). We integrate an advanced open-vocabulary, single-monocular 3D object detection tool that works with arbitrary camera views [43]. This tool not only detects a predefined set of common objects like cars, pedestrians, and traffic signs but its “open-vocabulary” nature also allows the model to dynamically specify new objects for detection based on the current scene’s needs, demonstrating remarkable flexibility and adaptability. The output from this tool provides indispensable input for subsequent trajectory prediction and risk assessment.

```
<tool_call>
  <tool_name>3D Object Detection</tool_name>
  <params>{"view_index": "front", "object_text": "barrier"}</params>
</tool_call>
```

Listing 4: Call Format of 3D Object Detection

6.3 DriveAlign-VQA Dataset Construction

To build a strong visual foundation for *DriveAgent-RI*, we constructed the DriveAlign-VQA dataset, a large-scale, high-quality collection of question-answer pairs specific to autonomous driving. The construction followed a systematic generation-and-validation pipeline, ensuring data diversity, relevance, and accuracy. The key stages are outlined below:

- 1. Image Collection and Diversification.** We first collected 1 million frames from real-world driving scenarios. To ensure a wide variety of scenes, we converted these images into CLIP embeddings, performed feature-based clustering, and then sampled a fixed number of images from each cluster. This process guarantees a diverse representation of road types, weather conditions, and traffic densities.
- 2. QA Pair Generation.** We employed the powerful Qwen2.5-VL-72B model to generate question-answer (QA) pairs from the curated images. The generation process used a mixed strategy: 70% of questions were derived from predefined templates covering key driving-related topics, while the remaining 30% were generated freely to capture more nuanced scene details (see the prompt below). The generation randomly utilized either a single front-view image or all six camera views to encourage robust, multi-perspective understanding.
- 3. Quality Validation and Filtering.** To ensure the highest quality, we used Doubao-Seed-1.6 as an automated “judge” model to validate every generated QA pair. The judge model scored each pair on dimensions such as question relevance, answer correctness, and grounding in visual evidence. Only pairs that received a perfect score were retained for the next stage.
- 4. Diversity Enhancement.** In the final step, we utilized Doubao-Seed-1.6 again to rewrite the validated questions. This step was crucial for increasing linguistic diversity and preventing the model from overfitting to specific phrasings in the templates. During this phase, we also filtered out overly simple or trivial QA pairs to maintain a high level of complexity in the final dataset.

This rigorous pipeline ultimately yielded the DriveAlign-VQA dataset, comprising 530K high-quality question-answer pairs that effectively develop driving-specific visual sensitivity in our base model.

Prompt for Free-Form VQA Generation

I am preparing high-quality visual question answering (VQA) training data to pretrain a Qwen2.5-VL-3B vision-language model (VLM) for autonomous driving scene understanding. For each input front-view driving scene image I provide, please strictly design four diverse and specific question-answer pairs based only on the visible content in the image. Your goal is to generate VQA data that focuses on the most crucial information for autonomous driving decision-making. Do NOT create any questions or answers about objects, events, or details that are NOT present in the given image. The questions should cover, as much as possible, the following critical aspects relevant to driving:

- Lane lines and road boundaries
- Presence, type, and status of traffic signs and lights
- Positions and number of vehicles, pedestrians, or cyclists
- Obstacles or unusual road conditions
- Road directions or upcoming maneuvers

For each image:

- Design 4 questions, each addressing a different key element visible in the scene.
- Provide an accurate and unambiguous answer to each question, strictly based on the image content.
- Do not invent information. Only output what can be directly observed.

Present your output as follows:

Q1: <question 1>
 A1: <answer 1>
 Q2: <question 2>
 A2: <answer 2>
 Q3: <question 3>
 A3: <answer 3>
 Q4: <question 4>
 A4: <answer 4>

Please begin when I input the first image.

6.4 DM-SFT CoT Data Construction Pipeline

To provide high-quality data for the initial SFT phase, we developed an automated data construction pipeline structured as a three-stage workflow (see Fig. 5). This pipeline systematically processes raw datasets—which exclusively contain multimodal inputs and ground-truth meta-actions—and converts them into comprehensive reasoning datasets that effectively integrate both $\mathcal{M}_{\text{tool}}$ and $\mathcal{M}_{\text{text}}$ reasoning modalities.

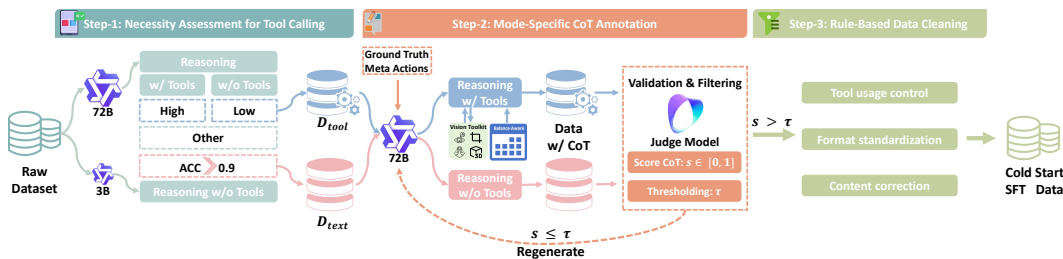


Figure 5: The automated three-stage pipeline for SFT data construction. The process consists of: (1) Necessity Assessment, which partitions data into tool-necessary D_{tool} and tool-unnecessary D_{text} sets; (2) Mode-Specific CoT Annotation, where a teacher model’s outputs are refined through a validation-regeneration loop with a judge model; and (3) Rule-Based Data Cleaning to produce the final dataset.

Step 1: Necessity Assessment for Tool Calling. This initial step partitions the raw dataset by discerning the necessity of tool use for each sample. Our two-model approach aims to establish clear boundaries for scenario complexity. We first employ a lightweight Qwen2.5-VL-3B model to filter out simple scenarios where high accuracy (e.g., > 0.9) is achievable in the $\mathcal{M}_{\text{text}}$ mode, forming the tool-unnecessary set D_{text} . For the remaining samples, a powerful Qwen2.5-VL-72B oracle model determines the tool-necessary set D_{tool} by identifying cases where the $\mathcal{M}_{\text{tool}}$ mode yields a significant performance gain over the $\mathcal{M}_{\text{text}}$ mode. This use of a highly capable oracle provides a reliable, conservative criterion for tool necessity, ensuring that we identify scenarios where external perception is genuinely beneficial, while leaving ambiguous cases for the exploratory set D_{explore} used in subsequent RL stages.

Step 2: Mode-Specific CoT Annotation and Validation. In this step, we generate mode-specific CoT annotations using the powerful Qwen2.5-VL-72B as the "teacher model." For each classified sample, the teacher model performs "inverse" reasoning from the ground-truth meta-actions to construct a logical thought process in either the $\mathcal{M}_{\text{text}}$ or $\mathcal{M}_{\text{tool}}$ mode. To ensure the quality and coherence of these annotations, we implement a rigorous validation and filtering process. A separate "judge model" scores the logical consistency of each generated CoT on a scale $s \in [0, 1]$. Samples with scores falling below a predefined quality threshold τ are automatically sent back to the teacher model for regeneration. This iterative refinement loop ensures that only high-fidelity reasoning paths are retained. To ensure a balanced distribution of tool use within the D_{tool} set, a **Dynamic Tool Preference Guidance mechanism** is also employed during this process, preventing a preference tool bias in the annotated data.

Step 3: Rule-Based Data Cleaning. In the final step, the annotated data is subjected to a rule-based cleaning pipeline to ensure its fidelity and uniformity. This pipeline performs three primary functions: (1) **Format Standardization**, which validates the structural integrity of the CoT and the syntactical correctness of tool calls; (2) **Content Correction**, which rectifies content-level errors such as annotation artifacts or mismatches between the final prediction and the ground-truth label; and (3) **Tool Usage Control**, which normalizes tool usage by constraining call frequency and eliminating redundant or illogical calls.

After this pipeline, we sample an equal number of high-quality instances from D_{text} and D_{tool} to construct the final cold-start SFT dataset, providing a solid foundation for the model’s hybrid-thinking capabilities.

6.5 Reward Design Details

Accuracy Reward (R_{acc}). The accuracy reward, R_{acc} , is designed to evaluate the quality of the generated meta-action sequence by comparing it to the ground-truth sequence. It is a composite score that combines the accuracy of speed and trajectory predictions, with a higher weight on speed to emphasize safety. The formulation is as follows:

$$R_{\text{acc}} = \lambda_s \cdot R_{\text{speed}} + \lambda_j \cdot R_{\text{traj}}$$

where $\lambda_s = 0.7$ and $\lambda_j = 0.3$ are the weighting factors for the speed reward (R_{speed}) and trajectory reward (R_{traj}), respectively.

Both R_{speed} and R_{traj} are calculated based on a weighted Levenshtein distance, which measures the similarity between the predicted sequence $\hat{A} = (\hat{a}_1, \dots, \hat{a}_m)$ and the ground-truth sequence $A = (a_1, \dots, a_n)$. The similarity score for a sequence is defined as:

$$R_{\text{seq}}(\hat{A}, A) = 1 - \frac{D(\hat{A}, A)}{\max(m, n)}$$

where $D(\hat{A}, A)$ is the weighted Levenshtein distance. The distance is computed recursively. Let $D(i, j)$ be the distance between the first i elements of \hat{A} and the first j elements of A . Then:

$$D(i, j) = \min \begin{cases} D(i-1, j) + C_{\text{del}} \\ D(i, j-1) + C_{\text{ins}} \\ D(i-1, j-1) + C_{\text{sub}}(\hat{a}_i, a_j, j) \end{cases}$$

The costs for deletion (C_{del}) and insertion (C_{ins}) are set to a constant value of 0.6 to allow for more flexible alignment between sequences of potentially different lengths. The substitution cost, C_{sub} , is defined as $1 - S(\hat{a}_i, a_j, j)$, where S is a position-aware match score:

$$S(\hat{a}, a, t) = \mathbb{I}(\hat{a} = a) \cdot w_{a,t}$$

Here, $\mathbb{I}(\cdot)$ is the indicator function, which is 1 if the predicted action \hat{a} matches the ground-truth action a , and 0 otherwise. $w_{a,t}$ is the **position-action weight** for the ground-truth action a at timestep t .

This weighting mechanism is designed to counteract the data imbalance. By up-weighting rarer, more critical actions (e.g., ‘‘Stop’’, ‘‘Left Turn’’), we encourage the model to learn a more balanced and robust decision-making policy. The weights are derived from the frequency $f_{c,t}$ of each action class c at each timestep t in the training data. The calculation proceeds in three steps:

1. **Raw Inverse Frequency Weight:** A raw weight $w'_{c,t}$ is calculated based on the inverse frequency relative to the mean frequency \bar{f}_t at that timestep, controlled by an exponent $\gamma = 0.5$:

$$w'_{c,t} = \left(\frac{\bar{f}_t + \epsilon}{f_{c,t} + \epsilon} \right)^\gamma$$

2. **Clipping:** The raw weights are clipped to a predefined range $[w_{\text{min}}, w_{\text{max}}]$ (e.g., $[0.7, 1.3]$) to prevent extreme values from destabilizing training:

$$w''_{c,t} = \text{clip}(w'_{c,t}, w_{\text{min}}, w_{\text{max}})$$

3. **Normalization:** Finally, the clipped weights for each timestep are normalized to have a mean of 1, ensuring that the weighting scheme adjusts the relative importance of actions without altering the overall scale of the reward at each timestep:

$$w_{c,t} = \frac{w''_{c,t}}{\frac{1}{|V|} \sum_{c' \in V} w''_{c',t}}$$

where V is the set of all possible actions for the given component (speed or trajectory).

This comprehensive reward design ensures that the agent is rewarded not only for correctness but also for learning to handle critical, less-frequent driving maneuvers effectively.

Tool Usage Reward (R_{tool}). In the final AMS-RL stage, the reward function is augmented with a tool-usage component, R_{tool} , to guide the agent in learning *when* to use tools. This reward is only applied to trajectories generated in the tool-use mode ($\mathcal{M}_{\text{tool}}$) and is designed to penalize superfluous tool calls while rewarding effective ones. The core mechanism is a **contrastive evaluation** within each group of G generated responses for a given input.

First, we establish a performance baseline, $\bar{R}_{\text{acc}}^{\text{ext}}$, by calculating the average accuracy of all text-only trajectories within the group. **If a group contains no such text-only paths, this baseline cannot be established, and the R_{tool} reward is not applied (i.e., set to zero) for that group, as no contrastive comparison is possible.** For groups where a baseline exists, the reward for each tool-assisted trajectory i is determined by its performance gain over this baseline, adjusted for a penalty corresponding to the number of tool calls.

The tool usage reward, R_{tool} , for a trajectory i that uses N_i tools is calculated as:

$$R_{\text{tool}} = (R_{\text{acc},i} - \bar{R}_{\text{acc}}^{\text{ext}}) - N_i \cdot C_{\text{tool}}$$

where $R_{\text{acc},i}$ is the accuracy reward of the current trajectory i , and C_{tool} is a small, constant cost per tool call (e.g., 0.01) that represents the computational overhead of active perception.

Finally, the reward is clipped to a fixed range, for instance $[-0.2, 0.2]$, to ensure training stability. This design explicitly incentivizes the agent to invoke active perception only when the accuracy improvement is significant enough to overcome the inherent cost of tool usage, fostering an intelligent and efficient decision-making process.

6.6 Training and Evaluation Prompt Template

Prompt Template for Model Training and Evaluation

<context>

You are provided with a front-view image of the car camera from the current frame.

The navigation command is: {navigation_command}.

Your current speed is: {speed} km/h.

<task>

Your task is to analyze the driving scenario, construct a natural, logical reasoning process and predict meta-actions. The following three stages are guidelines for structuring your thoughts:

1. <description>: Briefly describe the key aspects of the driving environment relevant to the decision. (<4 sentences)
2. <reasoning>: Briefly explain logically how the perceived situation helps you to predict the meta-actions. (<4 sentences)
3. <prediction>: Based on reasoning, briefly explain how you arrived at the meta-actions. (<2 sentences)

Finally, output the meta-actions for the current frame and the next 3 frames (2s interval between frames).

Output ONE composite action for each frame, each consisting of one speed token from {"Stop", "Keep Speed", "Accelerate", "Decelerate"} and one trajectory token from {"Left Turn", "Right Turn", "Straight"}.

Note that Left Turn and Right Turn include both major turns and minor adjustments like lane changes or small heading corrections.

<rule>

- Your response should be concise, prefer short, direct sentences.
- First check if context suffices for prediction, then choose <think_with_tools> or <think_no_tools>.

<tool_usage>

Under <think_with_tools>, you need to consider the following content:

- You are recommended to call the tools multiple times for better understanding (max 3 calls).
- Please call the tool meaningfully, as each call to the tool incurs additional costs.

Example:

```
<think_with_tools>(or <think_no_tools>)
  <description>
    ...(you can call tools here under <think_with_tools>)
  </description>
  <reasoning>
    ...(you can call tools here under <think_with_tools>)
  </reasoning>
  <prediction>
    ...(you can call tools here under <think_with_tools>)
  </prediction>
</think_with_tools>(or </think_no_tools>)
<meta actions>['Speed, Traj', 'Speed, Traj', 'Speed, Traj', 'Speed,
  Traj']</meta actions>
```

6.7 Automated Meta-Action Labeling Pipeline

To generate high-quality training labels, we developed a two-stage automated pipeline that converts raw vehicle trajectory data into discrete meta-action sequences. This pipeline first applies a set of

deterministic rules to generate initial labels and then leverages a VLM for refinement to handle complex or ambiguous cases.

Rule-Based Generation

The core of our pipeline is a rule-based labeling process that maps continuous trajectory data to a predefined vocabulary of speed and trajectory actions. This process is governed by a sliding window mechanism.

Sliding Window Mechanism. We employ a sliding window that spans a 3-second duration, encompassing 1 second of historical trajectory and 2 seconds of future trajectory relative to its center point. Starting from the current frame, the window slides forward four times in 2-second increments. This procedure generates a four-step discrete meta-action sequence, representing the planned behavior for the next 8 seconds at a 2-second resolution.

Trajectory-to-Action Mapping. For each segment of the trajectory captured by the window, we derive a composite meta-action consisting of a longitudinal (speed) and a lateral (trajectory) component based on the following rules:

- **Longitudinal Action (Speed):** The speed action is determined by the vehicle’s average speed and acceleration within the window.
 - **Stop:** If the speed is below a threshold of 0.5 m/s .
 - **Accelerate / Decelerate:** If the absolute acceleration exceeds a threshold of 0.3 m/s^2 .
 - **Keep Speed:** If the absolute acceleration is within the $\pm 0.3\text{ m/s}^2$ range.
- **Lateral Action (Trajectory):** The trajectory action is classified by calculating the overall angle between the initial and final direction vectors of the trajectory segment within the window.
 - **Straight:** If the absolute angle of deviation is less than 15° .
 - **Left Turn / Right Turn:** If the angle exceeds 15° , with the direction determined by the sign of the angle.

The thresholds for our rule-based labeling were determined based on domain knowledge and the physical plausibility of driving maneuvers to ensure the generated labels are both consistent and meaningful. Specifically, the speed threshold was set to 0.5 m/s (1.8 km/h), which is below typical pedestrian speed and effectively distinguishes intentional low-speed movements, such as creeping in dense traffic, from minor positional drifts or sensor noise that can occur when a vehicle is stationary. Complementing this, the acceleration/deceleration threshold of 0.3 m/s^2 represents a gentle but deliberate change in speed. Considering that the range for comfortable driving acceleration is significantly higher, typically $1.5 - 2.0\text{ m/s}^2$, our chosen value serves as a conservative lower bound for detecting intentional action. It was therefore chosen to separate a clear driver intent to alter speed from the subtle, often unconscious velocity adjustments made to maintain a constant pace during cruising, for instance, to counteract slight changes in road gradient. For lateral control, the heading change threshold of 15° over a 3-second window is used to differentiate the state of “driving generally straight” from any intentional lateral maneuver. A cumulative change of this magnitude signifies a conscious action to shift the vehicle’s trajectory, encompassing the full range of lateral actions—from minor corrective adjustments and lane changes to significant turns—and thereby cleanly separating them from the baseline action of proceeding straight. Collectively, these physically grounded thresholds provide a robust and interpretable mapping from continuous trajectory data to discrete behavioral actions.

VLM-Based Refinement

While our rule-based approach provides a consistent baseline for labeling, it can struggle with ambiguous or boundary cases where the trajectory is complex. To address this and enhance the quality of our labels, we introduce a VLM-based refinement stage. In this step, we leverage the advanced reasoning capabilities of GPT-4.1 to act as a proxy for human verification. We provide the model with a bird’s-eye-view (BEV) visualization of the ego-vehicle’s future trajectory alongside the initial rule-based meta-action sequence. The model is then tasked with evaluating the sequence for logical

consistency and correcting any discrepancies. This process ensures a higher fidelity of the final labels. The complete prompt used for this task is detailed below.

VLM Refinement Prompt

System Prompt:

You are an expert driving meta-action evaluator and corrector. You will be given a bird’s-eye-view (BEV) image where a blue polyline indicates the future ego trajectory. You will also receive a 4-step rule-based meta-action sequence, each step being a pair: [speed_action, trajectory_action]. Your job: (1) rate how consistent the sequence is with the visible trajectory shape and plausible driving behavior, (2) correct any unreasonable actions.

User Prompt:

Consider the image and the rule-based 4-step meta-action sequence.

- **Allowed speed actions:** Stop, Keep Speed, Accelerate, Decelerate.
- **Allowed trajectory actions:** Left Turn, Right Turn, Straight.
- Return a strict JSON object with keys: score (0-10 integer), reason, and final_meta_actions.
- final_meta_actions MUST be a list of EXACTLY 4 strings, preserving the original speed action for each step.
- Each string MUST be in the form ‘<speed>, <trajectory>’ using ONLY the allowed labels.
- **Temporal semantics:** the 4 steps cover [0-2s), [2-4s), [4-6s), [6-8s) after the current frame; the first step is the current 0-2s window.
- **Trajectory evidence:** ONLY use the first 16 future trajectory points starting from the current ego position; ignore farther points.
- **Global trend tolerance:** a turning trend does NOT require all steps to be turning; sequences like ‘Straight, Straight, Left Turn, Left Turn’ are acceptable.
- **Stationary cases:** if future points are nearly stationary (clustered at one location), DO NOT infer a turn; set the trajectory action to ‘Straight’ for those windows.
- **Plausibility filter:** only fix clearly unreasonable trajectory actions given the geometry and the 2s window (e.g., ‘Stop, Left Turn’ -> ‘Stop, Straight’).
- Do not add any commentary. Output only the JSON.

6.8 Human Evaluation Details

To establish a credible human performance benchmark, we recruited three licensed drivers, each possessing over two years of driving experience. The evaluation tasked these participants with the same high-level planning challenge assigned to the agent: predicting a sequence of four meta-actions for each driving scenario. To facilitate this, we developed a dedicated evaluation interface, as depicted in Figure 6. For each sample, this interface presented the forward-facing camera view, current vehicle speed, and the navigation directive. Participants then selected the appropriate meta-actions for the subsequent 8-second horizon using a series of dropdown menus. The test sets from both Drive-Interact and nuScenes were partitioned equally, with each participant evaluating a unique third of the samples. The final “Human” baseline score reported in the main results is the average of the accuracies from these three evaluators.

6.9 Extended Experimental Results

6.9.1 Detailed Results for Domain Alignment

To provide a comprehensive view of the benefits of our autonomous driving domain alignment strategy, this section presents the detailed performance breakdown of our *DriveAlign-3B* model. Table 7 compares its performance against the base model, Qwen2.5-VL-3B, and the larger Qwen2.5-VL-7B across our domain-specific DriveAlign-VQA_{test} benchmark and a suite of eight general VLM benchmarks.

Human Evaluation

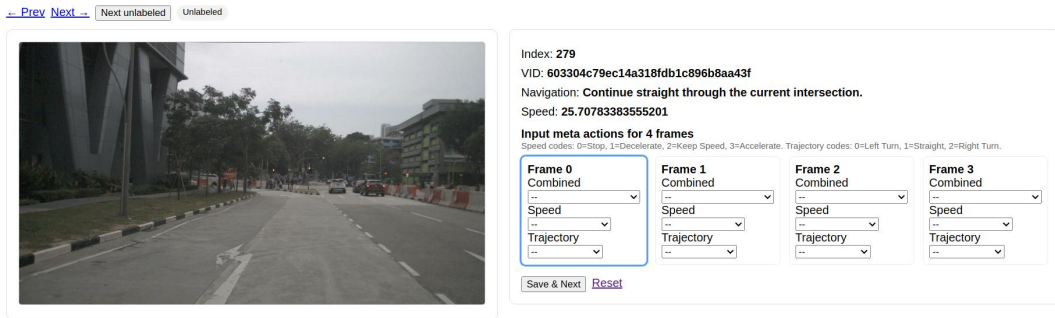


Figure 6: The user interface for human evaluation. For each scenario, evaluators were provided with the front-view camera image, a navigation instruction, and the current vehicle speed. They used the dropdown menus to predict the 4-step meta-action sequence for the upcoming 8-second interval.

As referenced in the main paper, the results demonstrate that *DriveAlign-3B* not only achieves a significant improvement of +11.7 points in the domain-specific overall score but also enhances its general VLM capabilities. This dual improvement validates our approach of developing robust driving-specific priors without compromising, and in many cases strengthening, the model’s foundational reasoning abilities.

Table 7: **Detailed results of domain alignment on in-domain and general abilities.** Scores on DriveAlign-VQA_{test} (upper) and 8 general VLM benchmarks (lower). Numbers in blue/red are deltas vs. Qwen2.5-VL-3B.

Task	Benchmark	DriveAlign-3B (ours)	Qwen2.5-VL-3B	Qwen2.5-VL-7B
DriveAlign-VQA _{test}	scene description	87.8 (+5.5)	82.3	82.2
	recognition of traffic entities	91.5 (+11.4)	80.1	86.4
	localization of critical targets	85.1 (+12.9)	72.2	67.9
	traffic commonsense and rules	74.0 (+17.1)	56.9	71.5
	overall	84.6 (+11.7)	72.9	77.0
General	MMStar	56.7 (+2.9)	53.8	60.6
	MMVet	60.6 (-0.6)	61.2	69.0
	MMBench_EN (val)	80.4 (+1.1)	79.3	79.7
	MMBench_EN_V11 (val)	77.4 (+1.0)	76.4	80.3
	MME-Realworld-lite	48.3 (+6.2)	42.1	44.6
	OCRBench	81.4 (-1.2)	82.6	88.1
	MMMU (val)	46.0 (+4.4)	41.6	48.4
	AI2D	80.1 (+1.9)	78.2	80.7
overall	66.4(+2.0)	64.4	68.9	

Notes. For DriveAlign-VQA_{test}, each of the four topics contains 200 samples; the judge model is Doubao Seed 1.6. The general benchmarks suite includes MMStar [44], MMVet [45], MMBench [46], MME-Realworld-lite [47], OCRBench [48], MMMU [49], and AI2D [50]. The general evaluation was performed using VLMEvalKit [51] with the default configuration.

6.9.2 Extended Ablation Results for Progressive Training Strategy

To further validate the robustness of our progressive training strategy, we present the ablation study results on the nuScenes dataset in Table 8. These results complement the main analysis conducted on the Drive-Internal dataset in Section 4.3.2. The performance trends observed on nuScenes are highly consistent with those on Drive-Internal, confirming that each stage of our training pipeline—from SFT to the cascaded FCM-RL and AMS-RL—contributes to a steady and significant improvement in the agent’s capabilities. This cross-dataset consistency underscores the general effectiveness and reliability of our proposed training methodology.

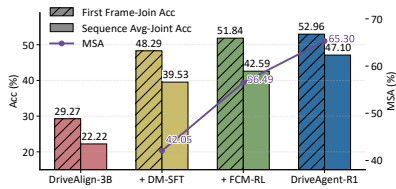


Figure 7: **Progressive training gains on nuScenes test set.** Accuracy in the adaptive mode ($\mathcal{M}_{\text{adaptive}}$) and MSA improve with each training stage.

Table 8: **Ablation on the progressive training strategy on the nuScenes test set.** We evaluate different combinations of our three training stages. To ensure fair comparison, we also test variants where a single RL stage (FCM-RL or AMS-RL) is trained for two epochs, matching the total RL epochs of our final model. Best results are in **bold**.

Variant	Training Stage			Sequence Avg-Joint Acc (%)			MSA (%)
	DM-SFT	FCM-RL	AMS-RL	$\mathcal{M}_{\text{test}}$	$\mathcal{M}_{\text{text}}$	$\mathcal{M}_{\text{adaptive}}$	
Variant-1 (SFT Only)	1 epoch	-	-	41.04	39.17	39.53	42.05
Variant-2 (+FCM)	1 epoch	1 epoch	-	42.92	40.58	42.59	56.49
Variant-3 (+FCM x2)	1 epoch	2 epochs	-	45.15	41.07	44.60	58.30
Variant-4 (+AMS)	1 epoch	-	1 epoch	41.18	40.58	40.92	57.76
Variant-5 (+AMS x2)	1 epoch	-	2 epochs	44.19	41.47	43.57	60.30
DriveAgent-RL (FCM→AMS)	1 epoch	1 epoch	1 epoch	46.38	44.43	47.10	65.30

6.10 Qualitative Results

This section presents qualitative examples to illustrate the capabilities of *DriveAgent-RL* in diverse driving scenarios. We begin with a simple case where the agent efficiently employs text-only reasoning (See Fig. 8 & Fig. 9). Subsequently, we showcase the agent’s active perception: at a busy intersection, it uses RoI Inspection and Retrieve View to check signals and pedestrian flow (See Fig. 10); in a low-visibility night scene, it leverages 3D Object Detection to uncover a hidden pedestrian (See Fig. 11); when approaching a barrier, the Depth Estimation tool provides the spatial awareness to navigate safely and plan ahead (See Fig. 12). Finally, two additional examples highlight the crucial role of RoI Inspection in resolving ambiguity by assessing the risk of distant pedestrians and confirming the state of a faraway traffic signal (See Fig. 13).

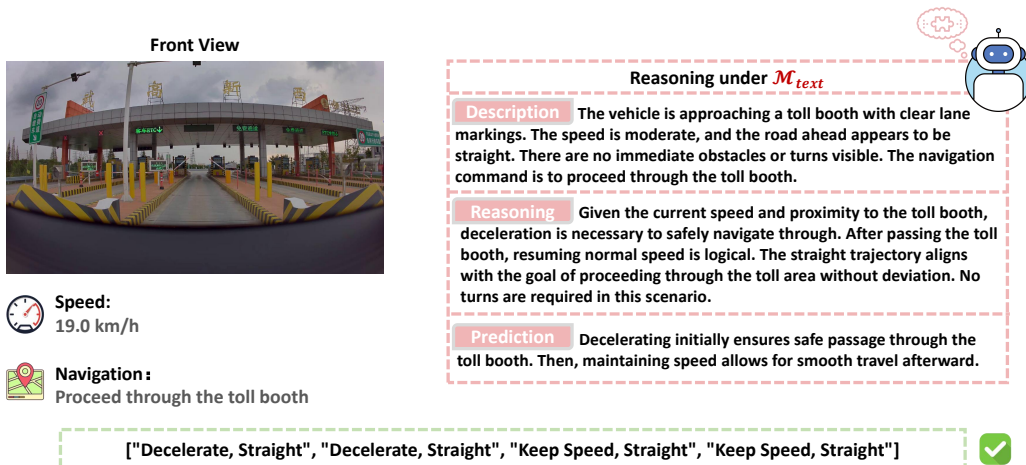


Figure 8: In this routine driving scenario, the vehicle approaches a toll booth with clear lane markings and straightforward navigation. Recognizing the low complexity and lack of ambiguity, *DriveAgent-RL* employs its efficient $\mathcal{M}_{\text{text}}$ mode. Through text-only reasoning, it formulates a safe and logical plan: decelerate to pass through the toll gate, then maintain speed to proceed, effectively handling a common situation without needing to invoke its vision toolkit.

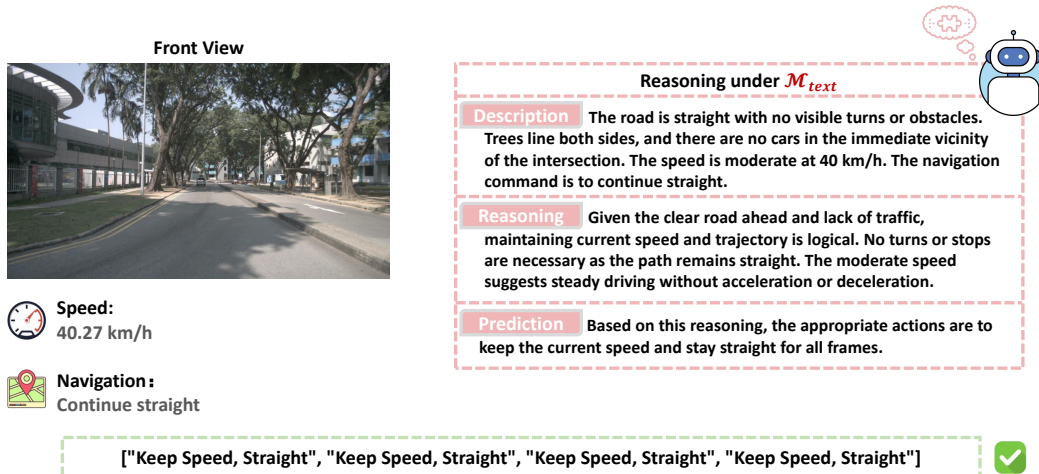


Figure 9: In this case, the road is straight and the view is open with no apparent obstacles, *DriveAgent-RI* engages its efficient text-only reasoning mode (\mathcal{M}_{text}) due to the low scene complexity. By solely analyzing the textual scene description and navigation command, it accurately assesses the simple road conditions and formulates a plan to “Keep Speed, Continue Straight.” This decision is made without invoking the vision toolkit, demonstrating the efficiency of the hybrid-thinking framework.

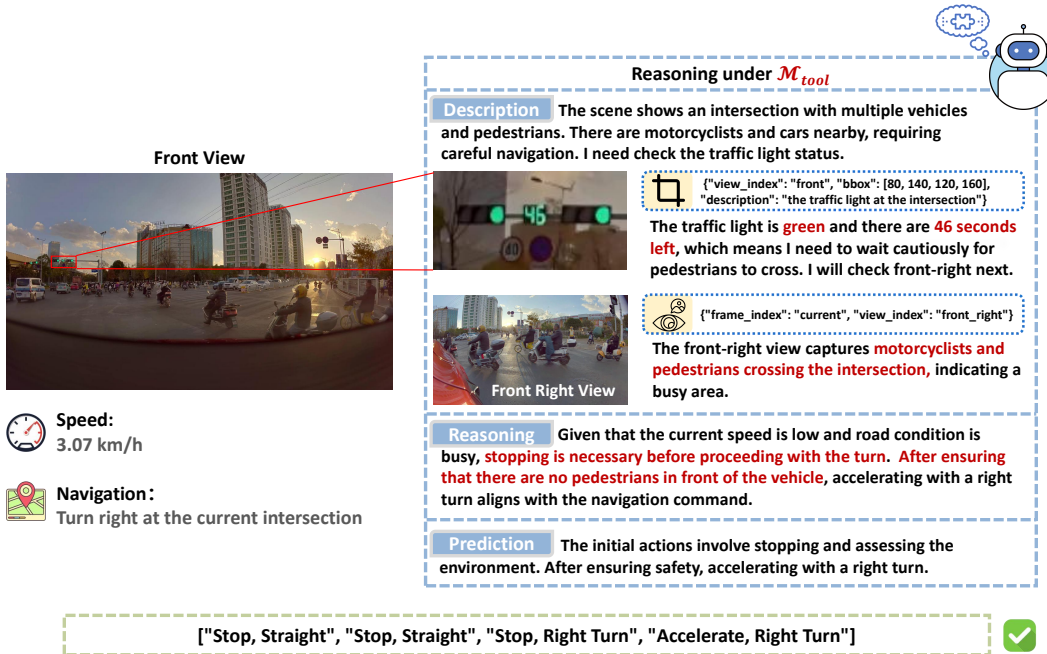


Figure 10: This case highlights the necessity of active perception when navigating a challenging right turn at a busy intersection with heavy pedestrian and motorcycle traffic. The initial view provides insufficient detail to ascertain the traffic light’s status, creating uncertainty. To resolve this, *DriveAgent-RI* proactively engages its \mathcal{M}_{tool} mode. It first invokes the “RoI Inspection” tool to confirm the green light and then use the “Retrieve View” to get the front-right view to better assess the dense flow of crossing traffic. By grounding its reasoning in this actively acquired visual evidence, the agent formulates a safe, context-aware plan: to stop and wait for pedestrians to clear before executing the right turn.

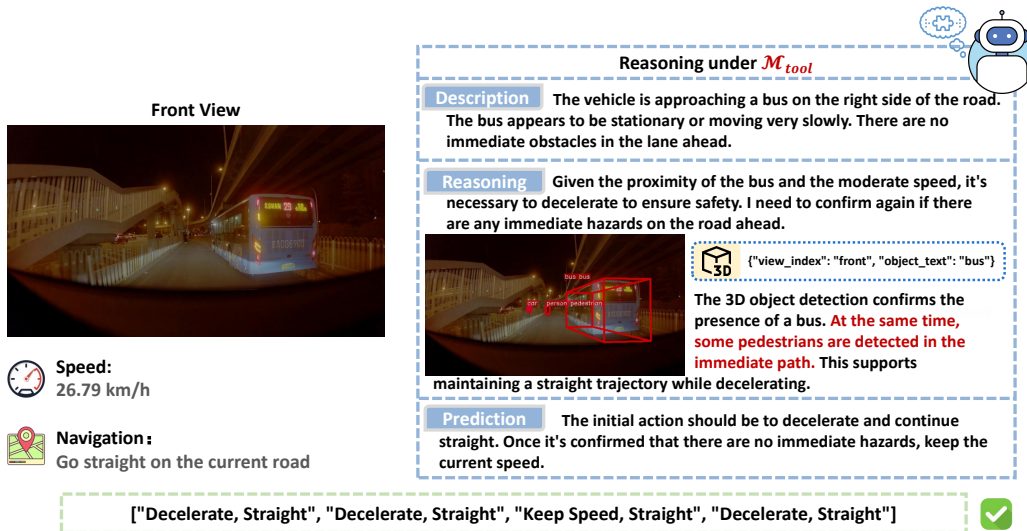


Figure 11: This case demonstrates the agent’s ability to uncover potential hazards in challenging low-visibility conditions. While navigating a narrow road at night, the initial perception identifies a nearby bus but fails to detect a pedestrian in the immediate path due to the darkness. By invoking the “3D Object Detection” tool, *DriveAgent-R1* performs active perception and successfully identifies the otherwise overlooked pedestrian. This critical, tool-grounded discovery prompts the agent to revise its initial assessment and decide to decelerate, prioritizing safety in response to the newly revealed risk.

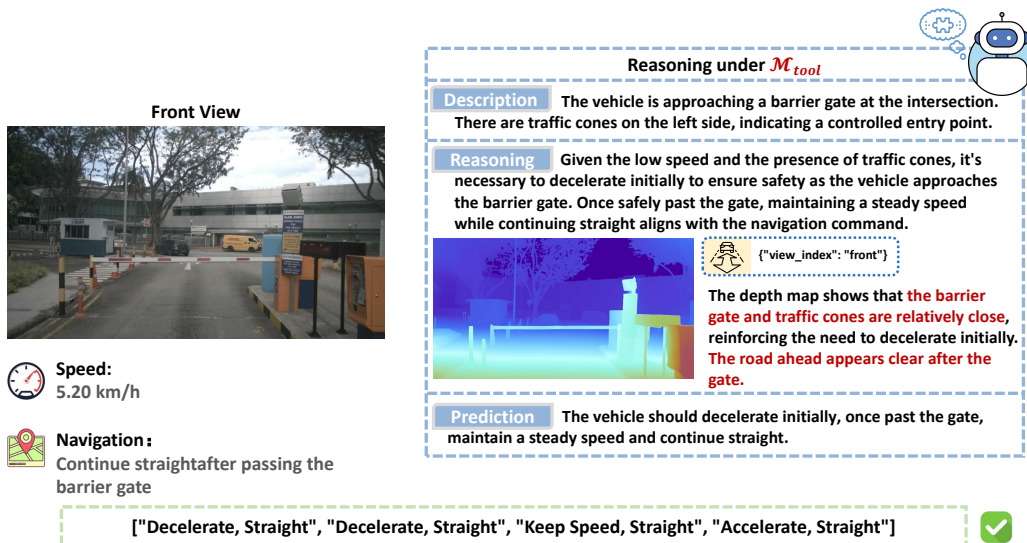


Figure 12: In scenarios requiring precise distance judgment, such as passing through this barrier gate, the “Depth Estimation” tool proves invaluable. The generated depth map provides two critical insights: it first confirms the gate’s close proximity, reinforcing the decision to decelerate for safe passage. More importantly, it also perceives the clear and open road beyond the barrier. This foresight into the upcoming environment allows *DriveAgent-R1* to formulate a confident, multi-stage plan: slow down to navigate the immediate obstacle, and then accelerate once safely through.

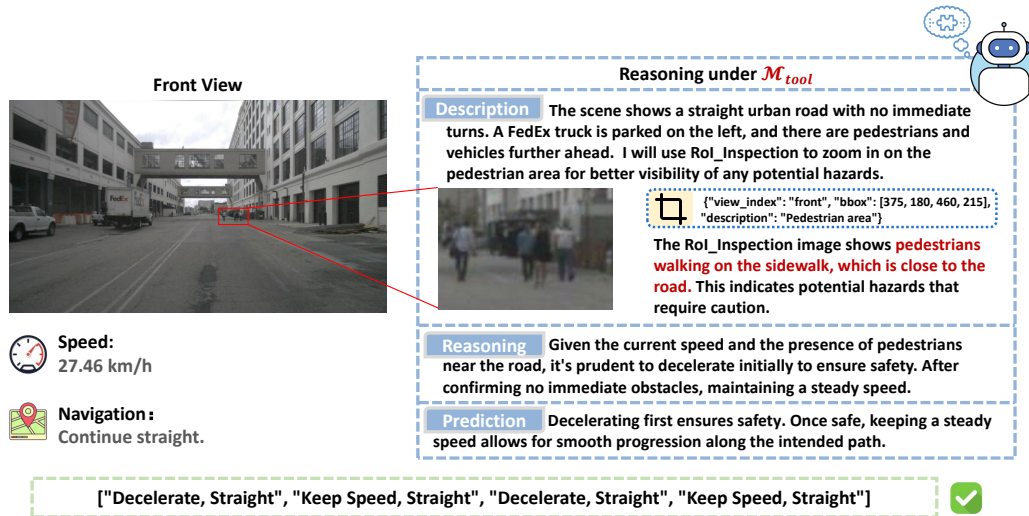


Figure 13: Even on a seemingly clear, straight road, *DriveAgent-RI* exhibits proactive caution by investigating distant activity. While the initial view shows pedestrians far ahead, their exact proximity to the road is uncertain. By deploying the “RoI Inspection” tool, the agent obtains a magnified view, revealing that the individuals are walking very close to the lane of travel. This specific, tool-acquired insight elevates the potential risk, prompting the agent to prudently decelerate to ensure a safe passage.

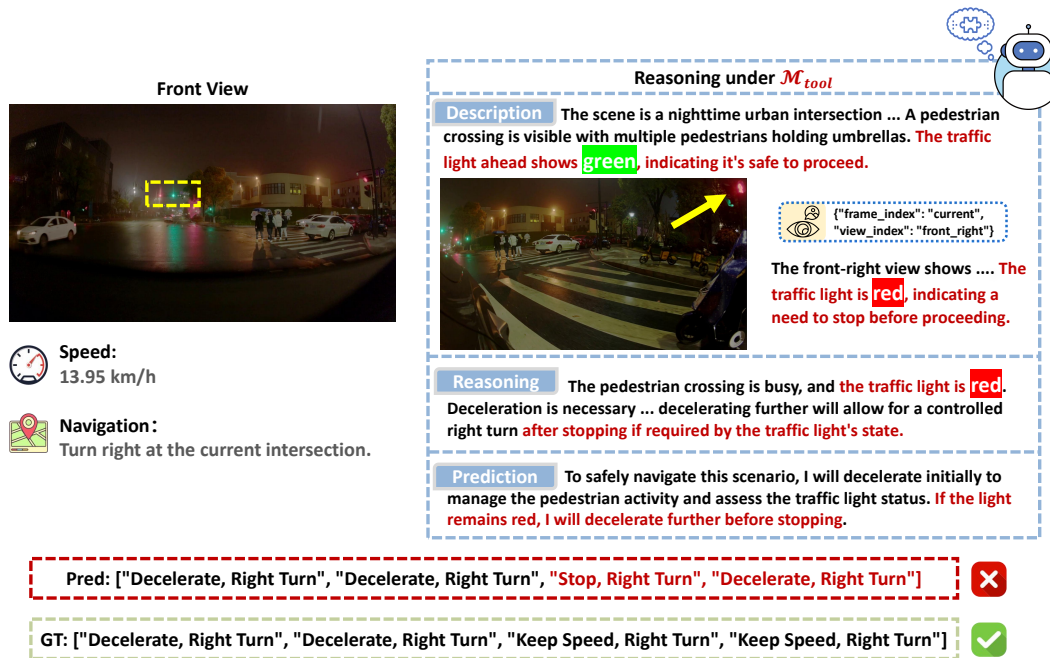


Figure 14: A failure case demonstrating incorrect traffic light identification. The agent initially correctly identifies the forward traffic light as green, but after retrieving a front-right view, it mistakenly focuses on the red pedestrian light, leading to an unnecessary “Stop” command in its final plan.

6.11 Analysis of a Failure Case in Complex Intersections

To provide a transparent assessment of our agent’s current limitations, this section analyzes a representative failure case in a complex urban intersection (see Figure 14). In this scenario, the agent initially correctly identifies its traffic light as green. However, after proactively retrieving a side-view

image to better assess the intersection, it misinterprets a red pedestrian signal as its own, causing it to override its correct initial judgment and erroneously plan to stop.

This failure highlights a key limitation: the agent's over-reliance on new visual evidence from its tools, which stems from an insufficient grasp of complex road topologies and traffic rules. Future work will directly address this challenge through two complementary directions: (1) strengthening the agent's foundational understanding of complex road topologies and traffic rules through targeted domain alignment, and (2) cultivating a more nuanced reasoning process capable of resolving informational conflicts. This will involve training the agent on adversarial scenarios with ambiguous visual cues, teaching it to weigh evidence and resolve contradictions rather than uncritically accepting the most recent perception. By implementing these measures, we aim to develop a more robust agent that not only actively perceives its environment but also critically reasons about what it sees, leading to safer and more reliable decision-making.